ACS OMEGA

Article

Cite This: ACS Omega 2018, 3, 12944−12955

http://pubs.acs.org/journal/acsodf

Conformational Disorder and Dynamics of Proteins Sensed by Raman Optical Activity

Carl Mensch,[†,‡] Patrick Bultinck,[‡] and Christian Johannessen*[,†]

[†]Department of Chemistry, University of Antwerp, Groenenborgerlaan 171, B-2020 Antwerp, Belgium

[‡]Department of Chemistry, Ghent University, Krijgslaan 281 (S3), B-9000 Ghent, Belgium

Supporting Information

ABSTRACT: Raman optical activity (ROA) spectra of proteins hold a lot of information about their structure in solution. To create a better understanding of the ROA spectra of, among others, the intrinsically disordered proteins (IDPs), involved in neurodegenerative diseases, the effect of conformational disorder and dynamics on the ROA spectra was studied. Density functional theory (DFT) calculations of small ensembles of model peptides with increasing disorder show that the ROA patterns of α-helical and polyproline II (PPII) structure reflect the average backbone angles in the ensemble. The amide III region in the ROA spectra of the α-helical peptides is shown to retain its typical −/+/+ pattern, while the amide III region of PPII secondary structure diminishes in intensity with increasing structural disorder. The results show that the ROA spectra of IDPs hence more likely stem from short stretches of well-defined PPII helices rather than a very flexible chain. Further DFT calculations support that mixing of PPII with helical secondary structure is consistent with experimental spectra of IDPs, while mixing with β-strand results in spectral patterns that are not observed experimentally. The detailed information obtained from these results contributes to a better understanding of the spectrum−structure relation.

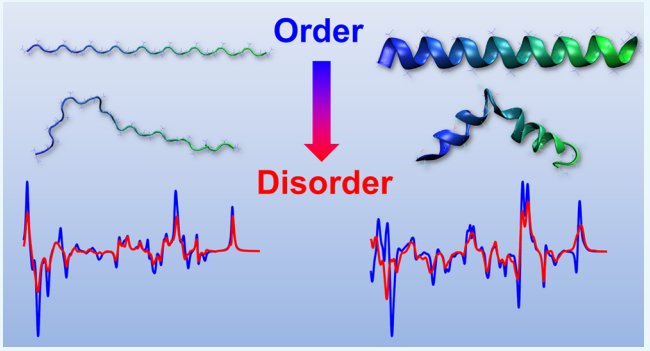

INTRODUCTION

Over the past decades, Raman optical activity (ROA) spectra have been shown to be uniquely sensitive to the solution structure of biomolecules.[1,2] Nevertheless, the use of ROA as a complementary structural elucidation technique in structural biology is not widespread. Exactly because of its strong structural sensitivity, the detailed interpretation of the spectroscopic signals is very challenging. Since ROA provides unique spectral patterns for inter alia peptides,[3] proteins,[1] glycoproteins,[4,5] and intrinsically disordered proteins (IDPs),[6,7] there is a clear incentive to create a deeper understanding of the structure−spectrum relationship. Especially proteins such as IDPs are challenging to characterize by standard techniques.[8] As these proteins are involved in neurodegenerative disorders such as Alzheimer's and Parkinson's disease, there is a strong motivation to develop structure elucidation techniques that are complementary to, for example, nuclear magnetic resonance (NMR) methodologies.[8]

The strength of Raman spectroscopies in the study of dynamic systems stems from the very short time scale of the scattering process (~3.3×10^{-14} s for a vibration with wavenumber 1000 cm^{-1}), which is much smaller than that of conformational changes.[9] The spectra are therefore a superposition of snapshot spectra arising from all conformations that the protein adopts in solution. Conventional Raman spectra of proteins arise from molecular vibrations in both the side chains and the backbone of the protein. ROA on the other hand is a chiroptical technique as it is measured as the difference in the right- (I_R) and left-handed (I_L) circularly polarized components in Raman scattered light. Because of its sensitivity to chirality, ROA mainly records signals from the most rigid parts of the protein. Therefore, the experimentally observed ROA spectral patterns mainly arise from amide bond and skeletal stretching vibrations in the backbone of the protein and thus depend on the secondary structure of the protein.[1] While the most important secondary structure elements such as α-helix and β-sheet can readily be identified from a protein's ROA spectrum, the detailed interpretation of ROA spectra is elusive.[10] Therefore, in the past decade, several studies have been performed using density functional theory (DFT) to calculate Raman and ROA spectral patterns to aid in the interpretation of the experimental patterns.[11,12] Both for peptides[3,13,14] and proteins,[15−18] the interpretation of the experimental spectra based on DFT calculations has been reported. In other approaches, DFT calculations of model systems such as poly-L-alanine peptides were used to support the general understanding of the relationship between protein structure and the ROA spectrum.[19−24]

Received: August 9, 2018
Accepted: October 3, 2018
Published: October 10, 2018

DOI: 10.1021/acsomega.8b01955
ACS Omega 2018, 3, 12944−12955

Recently, our group has reported the creation of an ROA database to study the relationship between the secondary structure and the corresponding ROA patterns.[10] This database consists of a large collection of ROA spectra, each one calculated for a HCO-(L-Ala)$_5$-NH$_2$ or a HCO-(L-Ala)$_{11}$-NH$_2$ peptide with all ϕ backbone torsion angles set to the same value and all ψ angles set to the same value. By selecting a large number of geometrically possible combinations of ϕ and ψ angles, a collection of regular conformations with the corresponding spectra was created. Using that database, the experimental ROA patterns of various peptides adopting a specific secondary structure in solution could be elucidated.[10] Interestingly, the database also correctly assigns the secondary structure of the flexible XAO peptide that has an important conformational propensity to poly-L-proline type II helix (PPII), yet is considered to be flexible and explore multiple regions of the Ramachandran space.[10,25] A PPII helix is characterized by the backbone ϕ and ψ torsion angles clustering around ϕ = −75° and ψ = 145° in the Ramachandran plot and is also observed for sequences that do not contain proline.[25] It is an important secondary structure element of both globular proteins and flexible and dynamic IDPs.[25] Since our ROA database[10] considers only fixed model geometries with a regular arrangement of backbone torsion angles (the same ϕ and the same ψ angles for each residue in the backbone), it would conceptually be less useful to study IDPs compared to well-ordered peptides. Given the need to further understand the effect of conformational dynamics and disorder on the ROA spectra of peptides and proteins, we here extend the database to account for structural disorder. To this end, using DFT, the ROA spectrum was first computed for a peptide model with a fixed backbone conformation by setting the ϕ and ψ angles of all residues in its sequence to the same values across the backbone. Next, the effect of conformational dynamics and disorderedness was investigated by increasingly deviating the conformation of this peptide from the original regular conformation and monitoring its effect on the computed ROA spectrum. In this study, the effect of conformational dynamics on the ROA spectra of the left-handed PPII helix and the right-handed α-helix was studied, since ROA has been shown to be very sensitive to these types of secondary structure, yet the detailed understanding of their spectral characteristics is still lacking.[10] Furthermore, these secondary structure types are of interest to elucidate the experimental ROA spectra of IDPs.[7]

RESULTS AND DISCUSSION

Intrinsic Disorder and the PPII Secondary Structure.

IDPs are very flexible proteins, but many of their backbone torsion angles fluctuate around ϕ = −75° and ψ = 145°, characteristic for PPII secondary structure.[25] ROA gives unique spectral patterns of IDPs that support that these dynamic proteins do not merely behave like random coils but do contain residual structure.[7,21,26] The most prominent band (∼1320 cm^{-1}) in the experimental ROA spectra of IDPs is assigned to PPII secondary structure, although further understanding of the relation between the spectral patterns and a protein's structure is lacking.[1,21,27] Recently, our group has reported the experimental ROA spectrum of the XAO peptide that is considered to primarily adopt PPII helical structure.[10,25,28,29] Yet, the XAO peptide is flexible and its radius of gyration was shown by small-angle X-ray scattering to be much smaller than that it would be for a fully extended PPII helix.[29] Zhu et al. suggested that this observation of a low radius of gyration could be reconciled with the strong evidence from spectroscopic methods pointing to a major contribution of PPII helical structure in the peptide, by proposing that flexible stretches of PPII structures are truncated by other secondary structure elements.[21,25] We showed that the experimental ROA spectrum of the XAO peptide was very well reproduced by spectra calculated using DFT of poly-L-alanine model structures with a regular PPII backbone conformation, i.e., with all backbone torsions set to ϕ = −75° and ψ = 145°.[10] This observation hence prompted us to further study how the spectral patterns would be affected by conformational dynamics or disorder, as both the XAO peptide and IDPs in general have a dynamic and flexible structure, although with a propensity for PPII conformation. To account for the increased flexibility, we generated sets of structures with $\phi \pm \sigma$ and $\psi \pm \sigma$ based on chosen values for σ (Scheme 1). Four families of 50 structures were defined with σ = 6, 10, 20, or 30. The Ramachandran plots in Figure 1a show the distribution of the torsion angles going from ϕ = −75° ± σ and

Scheme 1. By (1) Choosing a Pair of ϕ and ψ Angles, (2) a Regular Structure Is Created, in Which All Backbone ϕ and ψ Angles Are Equal to the Chosen Pair of Angles; (3) Conformational Disorder Is Introduced by Deviating the Original Pair of Angles More and More by Using a Different Normally Distributed Random Number σ_{τ,c_k} for Each Torsion Angle ("randn" in Matlab).

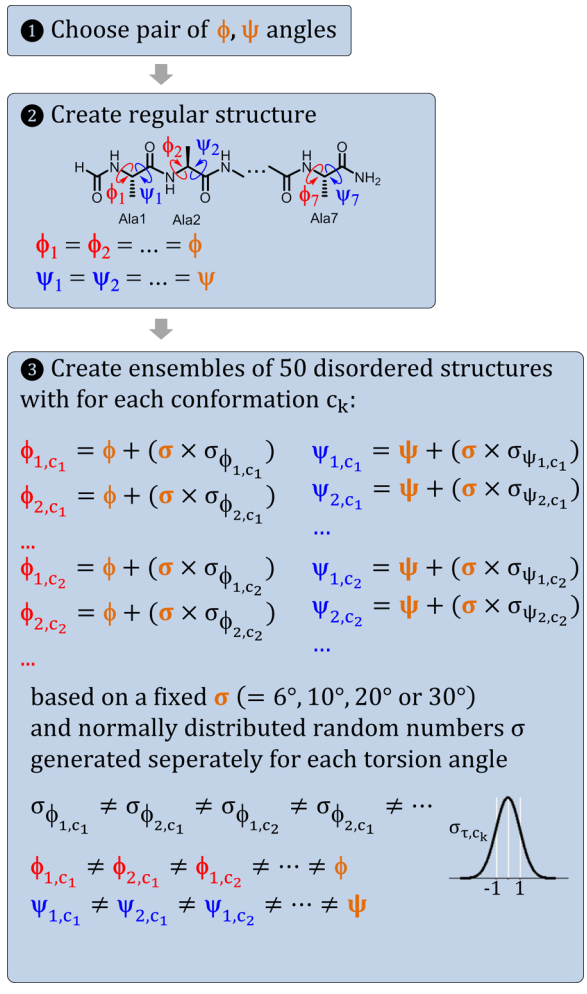

DOI: 10.1021/acsomega.8b01955
ACS Omega 2018, 3, 12944−12955

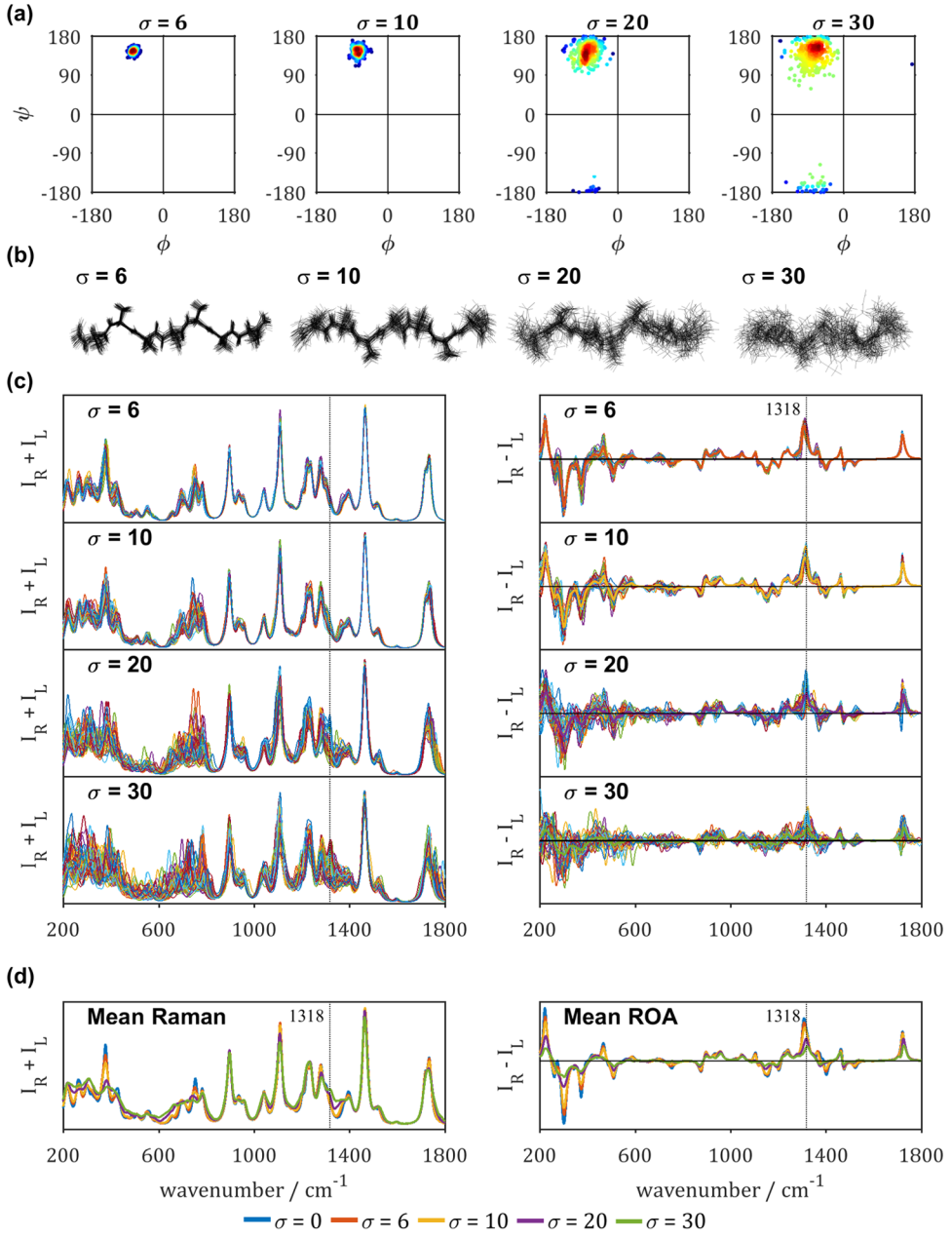

Figure 1. Effect of conformational disorder on the Raman and ROA patterns of PPII secondary structure. The backbone conformation of HCO-(L-Ala)$_7$-NH$_2$ is increasingly randomized by deviating each ϕ and ψ angle in the backbone from $\phi = -75°$ and $\psi = 145°$ to $\phi = -75° \pm \sigma$ and $\psi = 145° \pm \sigma$ in steps of $\sigma = 6$, 10, 20, 30. (a) Ramachandran plots displaying the increasing deviation from the mean angles $\phi = -75°$ and $\psi = 145°$ for each family of 50 structures with a set standard deviation σ. (b) Superposition of the 50 random conformations of HCO-(L-Ala)$_7$-NH$_2$ shown as stick figures for each family. (c) Individual Raman ($I_R + I_L$) and ROA ($I_R - I_L$) spectra of each family of 50 conformations. (d) Mean Raman and ROA spectra of the four families with $\sigma = 6$ (red), 10 (yellow), 20 (purple), or 30 (green) compared to the computed spectrum of HCO-(L-Ala)$_7$-NH$_2$ with all backbone angles set to $\phi = -75°$ and $\psi = 145°$ (blue; $\sigma = 0$).

$\psi = 145° \pm \sigma$ with a low standard deviation from the mean angles ($\sigma = 6$) to much more conformationally randomized structures ($\sigma = 30$). The Ramachandran plots show all ϕ and ψ backbone angles of the 50 conformations of each conformational family. The corresponding molecular geometries are displayed as superimposed stick figures in Figure 1b. In the Raman and ROA spectra, the largest variation is observed in the lower-wavenumber region (200−800 cm^{-1}) and the extended amide III region (1240−1345 cm^{-1}), as shown in Figure 1c. Although the individual spectra are distinctly different, averaging of the spectra over the 50 conformations in each family leads to mean spectra with similar patterns. In Figure 1d, the Raman and ROA spectra of HCO-(L-Ala)$_7$-NH$_2$ with all backbone angles set to $\phi = -75°$ and $\psi = 145°$ (blue, $\sigma = 0$) are compared to the mean spectra of the four conformational families ($\sigma = 6$, 10, 20, and 30 in red, yellow, purple, and green, respectively). The Raman spectral patterns are affected only to a very limited extent by the increasing conformational disorder. The most apparent changes are the broadening of the lower-wavenumber region (200−800 cm^{-1}), which leads to the lowering of the band maxima in that region.

ROA is more sensitive to the increase in conformational freedom. Both the low-wavenumber region and the extended amide III region in the ROA spectra are strongly reduced in

DOI: 10.1021/acsomega.8b01955
ACS Omega 2018, 3, 12944−12955

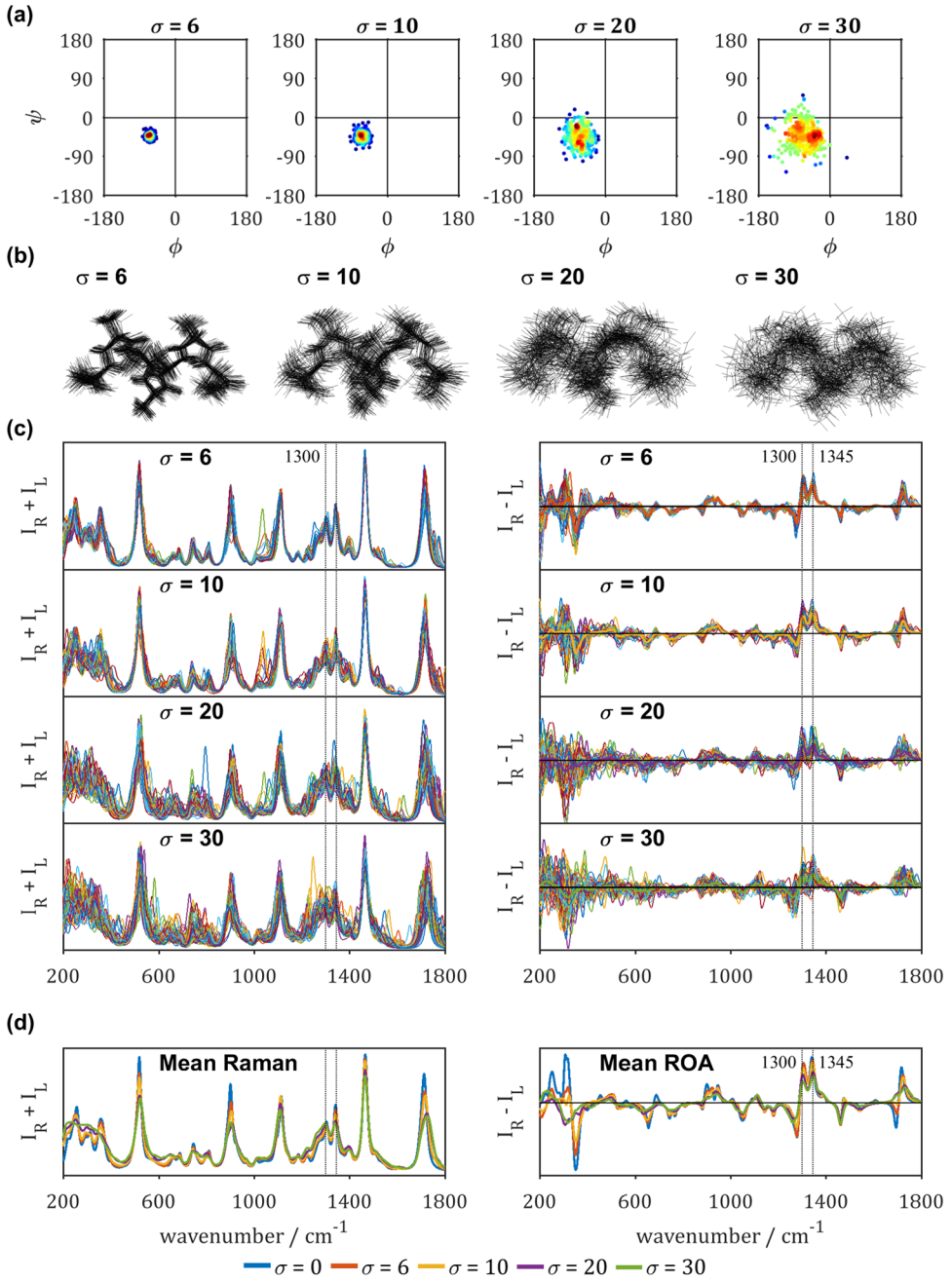

Figure 2. Effect of conformational disorder on the ROA patterns of α-helical secondary structure. The backbone conformation of HCO-(L-Ala)$_7$-NH$_2$ is increasingly randomized by deviating each ϕ and ψ angle in the backbone from $\phi = -66°$ and $\psi = -41°$ to $\phi = -66° \pm \sigma$ and $\psi = -41° \pm \sigma$. (a) Ramachandran plots displaying the increasing deviation from the central $\phi = -66°$ and $\psi = -41°$ angles for each family of 50 structures with a set standard deviation σ. (b) Superposition of the 50 conformations of HCO-(L-Ala)$_7$-NH$_2$ shown as stick figures for each conformational family. (c) Individual Raman ($I_R + I_L$) and ROA ($I_R - I_L$) spectra of each family of 50 conformations. (d) Mean Raman and ROA spectra of the four families (σ = 6 (red), 10 (yellow), 20 (purple), and 30 (green)) compared to the computed spectrum of HCO-(L-Ala)$_7$-NH$_2$ with all backbone angles set to $\phi = -75°$ and $\psi = 145°$ (blue; $\sigma = 0$).

intensity with increasing conformational disorder of the HCO-(L-Ala)$_7$-NH$_2$ model peptide. The ratio of the maximum intensity of the amide III relative to the amide I region is also reduced as the maximum intensity of the amide III region drops significantly with increasing disorder. This suggests that the relative ratio in experimental spectra of IDPs could be used as an indicator of the dynamics or conformational freedom of IDPs. For example, both the XAO peptide[10] (see above) and the IDP α-synuclein[7] in their experimental ROA spectra have a positive amide III band with a maximum intensity that is higher relative to the amide I maximum intensity. The ROA spectra in Figure 1 hence suggest that the standard deviation of the mean torsion angles of XAO and α-synuclein in the PPII region of the Ramachandran plot does not exceed $\sigma = 20$. This suggests that the ROA patterns of IDPs arise from short sequences in the protein adopting PPII conformation with torsion angles very close to $\phi = -75°$ and $\psi = 145°$. Our results support the hypothesis that the XAO peptide adopts PPII helical secondary structure truncated by other secondary structure elements and furthermore indicate that the variation

DOI: 10.1021/acsomega.8b01955
ACS Omega 2018, 3, 12944−12955

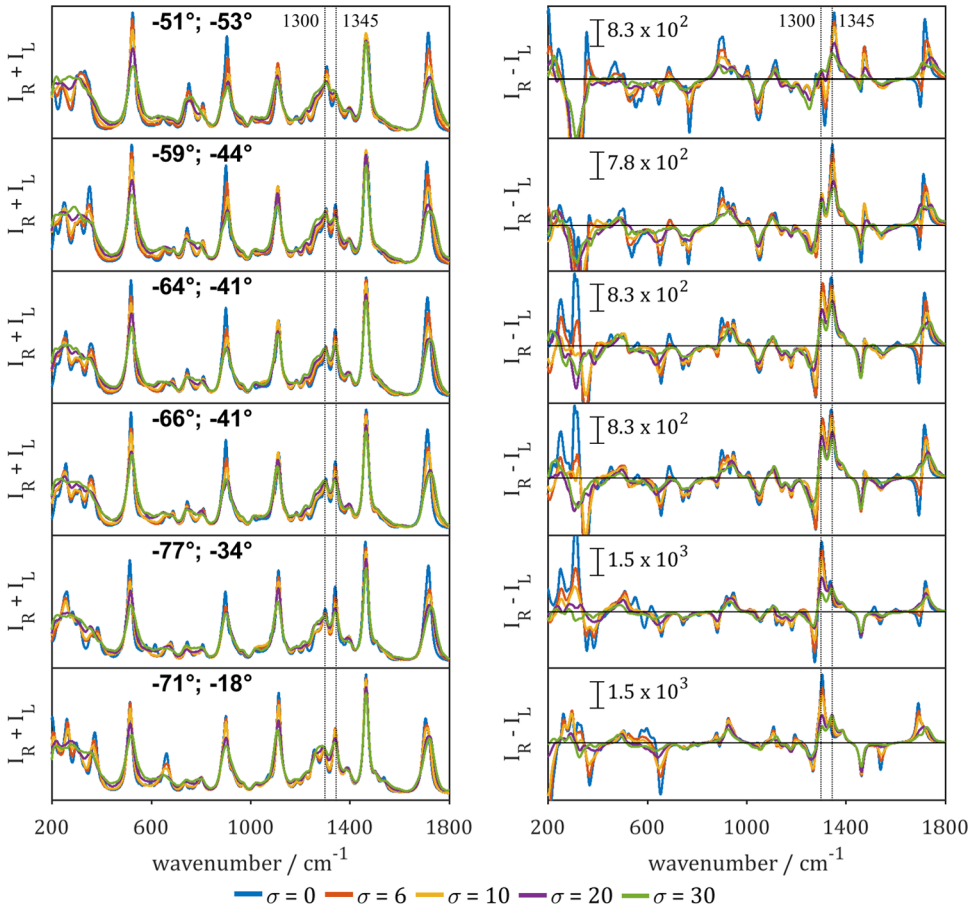

Figure 3. Effect of conformational disorder on the ROA patterns of right-handed helical secondary structure. For six couples of ϕ and ψ angles, the conformation of HCO-(L-Ala)$_7$-NH$_2$ was increasingly randomized by deviating each ϕ and ψ angle in the backbone from the initial ϕ and ψ to $\phi \pm \sigma$ and $\psi \pm \sigma$ in families of 50 conformations with respective standard deviation σ (see Scheme 1). Mean Raman ($I_R + I_L$) and ROA ($I_R - I_L$) spectra of HCO-Ala$_7$-NH$_2$ with backbone torsion angles set to various values corresponding to α-helical secondary structure or 3_{10}-helix (σ = 0; blue) and the deviation from that with torsion angles with a standard deviation from these angles set to σ = 6 (red), 10 (yellow), 20 (purple), and 30 (green). The red, yellow, purple, and green spectra correspond to the average of 50 spectra of the family of 50 model structures with randomly generated normal distributed torsion angles.

of the backbone angles in the PPII region of the Ramachandran plot is limited.

To further investigate the effect of mixing different secondary structure elements, in the following sections, the effect of mixing PPII secondary structure with right-handed helical structure is evaluated. Before this mixing can be considered, in the next section, we first examine how the ROA patterns of α-helical structure on its own are affected by increasing conformational disorder.

ROA Patterns of Right-Handed Helical Structure. The ROA bands that mark α-helical protein structure are well studied and were assigned years ago.[1,30] The most distinctive patterns are a −/+ couplet centered at ∼1650 cm^{-1} in the amide I region and a −/+/+ pattern at ∼1245/1300/1345 cm^{-1} in the extended amide III region.[1,10] The relative ratios of the amide III bands of α-helical proteins differ, which therefore has been suggested to be sensitive to the precise ϕ and ψ angles. However, the detailed interpretation has been a matter of debate in the scientific literature. Already in 1999, Blanch et al. suggested that the positive band around 1345 cm^{-1} (Cα−H bending vibration parallel to the C−N bond, coupled with amide III) marks hydrated helical structure, while the 1300 cm^{-1} (Cα−H bending vibration perpendicular to the C−N bond, coupled with amide III) was proposed to be a signature of α-helical structure without hydration.[10,31,32] These assignments were later questioned and shown to be inaccurate.[10] Nevertheless, our group showed that the ratio of the two bands is very sensitive to the exact helical geometry, which can be affected by intramolecular hydrogen bonding or interaction with the solvent.[10] The database developed in our group showed that helical structure with the C═O group tilting outward from the helix axis gives rise to a very intense ROA band around 1300 cm^{-1}, while the band around 1345 cm^{-1} is a conservative marker of α-helical structure. Since that database consists of regular conformations with repeated ϕ and ψ angles, here the influence of conformational dynamics on the ROA patterns of α-helical structure was investigated. In Figure 2, the spectra of the HCO-(L-Ala)$_7$-NH$_2$ model peptide in an α-helical conformation with typical backbone torsion angles ϕ = −66° and ψ = −41° are shown and how the Raman and ROA patterns are affected when these specific torsion angles are increasingly randomized. As shown in Figure 2a,b, with high standard deviations σ of the mean ϕ and ψ angles, the regular α-helical structure is very much randomized from the regular conformation. Because of that, both the Raman and ROA spectra of the individual conformations in each family are strongly affected, as shown in the superimposed spectra in Figure 2c. It is therefore a striking result that the mean spectra

DOI: 10.1021/acsomega.8b01955
ACS Omega 2018, 3, 12944−12955

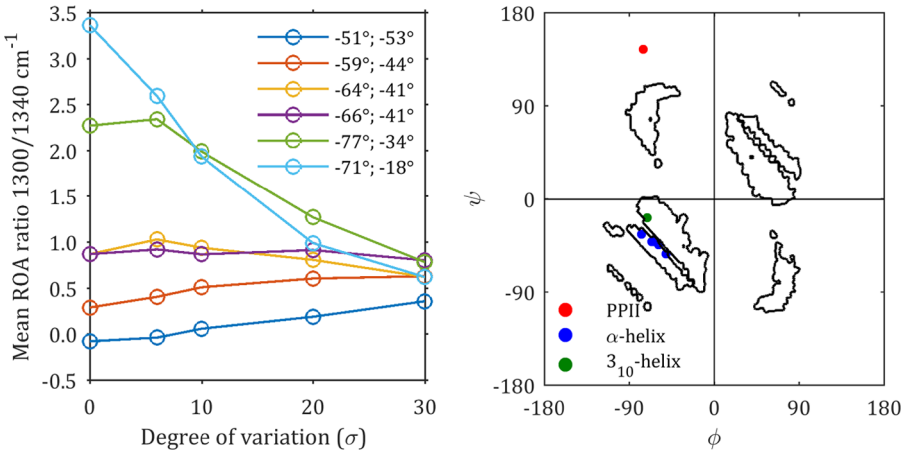

Figure 4. (Left) Ratio of the maximum intensity of the two positive bands in the extended amide III region of the mean ROA spectra at 1300/1345 cm^{-1}. (Right) Ramachandran plot showing the (ϕ; ψ) pairs of angles used in this study: (−75; 145°), (−51; −53°), (−59; −44°), (−64; −41°), (−66; −41°), (−77; −34°), (−71; −18°). The contour lines mark different secondary structure regions based on the hydrogen bonding in regular model alanine heptapeptides (see ref 10).

of each family of conformations are so similar (see Figure 2d). The largest spectral differences in the mean spectra are observed in the lower-wavenumber region that drops significantly in maximal intensities and in the amide I region, which loses the negative portion of the characteristic −/+ couplet. As we showed before that the amide III region is very sensitive to the exact α-helical conformation,[10] it is a remarkable result that the mean patterns here are so similar. While the individual spectra shown in Figure 2c show a lot of variation in that region, the mean spectra show the same relative intensities of the −/+/+ pattern.

ROA Is Sensitive to the Mean α-Helical Conformation. As our previous work showed that ROA is very sensitive to the exact α-helical conformation,[10] the results shown in Figure 2 were extended to other α-helical conformations (specific pairs of ϕ and ψ angles) to study the effect of conformational disorder in more detail. Similar to the results discussed above, first, the ROA spectra of regular HCO-Ala$_7$-NH$_2$ model conformations with all ϕ and ψ backbone angles equal were computed. The computed Raman and ROA spectra are shown in Figure 3 by the blue lines and thus correspond to a Raman and an ROA spectrum of a single conformation. By looking at five different pairs of ϕ and ψ angles, the effect of slight differences in the α-helical conformation is evaluated. These results are also compared to a 3_{10}-helical conformation ($\phi = -71°$ and $\psi = -18°$) to confirm the structural sensitivity of ROA to different types of helix. The red, yellow, purple, and green lines correspond to the average spectra of families of 50 structures with the standard deviation σ of the mean ϕ and ψ backbone angles being σ = 6, 10, 20, and 30, respectively (see Figures S1−S5 for the spectra of the individual conformations).

The mean Raman spectra in Figure 3 mostly show broadening of the spectral patterns with increasing conformational disorder (higher σ) from the original regular helix conformation (blue; σ = 0). The spectral differences in the mean ROA spectra are similar to those observed in Figure 2. Also for the other α-helical conformations, the amide I region in the ROA spectra in Figure 3 does not show the negative contribution of the couplet upon increasing conformational disorder. Since for α-helical proteins and peptides the amide I is always observed as a −/+ couplet, this indicates that this spectral pattern arises from regular helical structure with a limited variation of the backbone ϕ and ψ angles.

In accordance with our previous analysis,[10] the spectra of the α-helical models with slightly different mean backbone angles show markedly different amide III patterns. We showed that the ratio of the maximal intensity of the positive amide III bands depends on the ϕ and ψ angles in the backbone of regular α-helical model conformations. For α-helical conformations defined by torsion angles in the bottom right of the α-helical region in the Ramachandran plot to the top right in that same region, the intensity of the ROA band around 1300 cm^{-1} relative to the band around 1345 cm^{-1} increases. The band around 1345 cm^{-1} was shown to be a conservative marker of α-helical structure. This is also observed in Figure 3, by comparing the ROA spectra of the same color. For example, the blue spectra of the top three panels show a much higher positive maximum intensity around 1345 cm^{-1}, relative to the 1300 cm^{-1} band, compared to the ratio in the panels below.

The effect of increasingly deviating the conformation from the regular conformation (all ϕ angles and all ψ angles equal, see Scheme 1) can be seen by comparing the ROA spectra within the same panel from σ = 0 (blue) to σ = 30 (green). Very surprisingly, the amide III region of the α-helical models is robust with the increase in variation of the backbone conformation; in other words, the −/+/+ pattern and relative ratios remain generally the same for each combination of ϕ and ψ angles. This shows that the amide III region of α-helical proteins is a pattern resulting from the average helix conformation in the structural ensemble. In agreement with our previous results, the positive band around 1345 cm^{-1} is a robust marker of α-helical structure; it is found in all calculated spectra of α-helical structure, even if the helix is considerably random (see spectra for σ = 20 or 30). The positive band around 1300 cm^{-1} is very sensitive to the combination of ϕ and ψ angles and has a very low (even negative) value for structures with backbone angles in the bottom right of the α-helical region of the Ramachandran plot and gradually increases for structures with backbone angles toward the top left of the α-helical region (see Figure 3 and ref 10).

These observations are further supported by analyzing the ratio of the maximum intensity of the two positive bands at 1300 and 1345 cm^{-1} in the amide III region in Figure 4. In

DOI: 10.1021/acsomega.8b01955
ACS Omega 2018, 3, 12944−12955

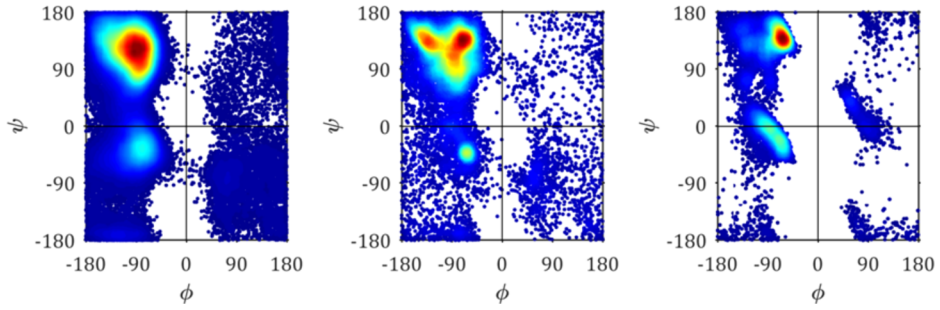

Figure 5. Ramachandran plots of the α-synuclein ensembles by Allison et al. (left), Tóth et al. (middle), and Schwalbe et al. (right).[33−35]

agreement with our earlier results, the ratio is very sensitive to the exact combination of the ϕ and ψ angles, observing very high ratios for structures with backbone angles in the top left of the helical region in the Ramachandran plot, to much lower ratios in the bottom right. Both for the α-helical model with torsion angles set $\phi = -77°$ and $\psi = -34°$ and the 3_{10}-model with $\phi = -71°$ and $\psi = -18°$, the positive band around 1300 cm^{-1} has a very high intensity that collapses with increasing conformational freedom.

Only with a very high degree of conformational dynamics or disorder (σ = 30), all helical models, including the 3_{10}-conformation, obtain a similar ROA pattern (Figure 3) and intensity ratio (Figure 4). To conclude the above results, the intensity ratio of the two bands is sensitive to the average helical conformation.

Effect of Mixing PPII with Other Secondary Structures on the ROA Patterns. As discussed above, IDPs adopt a substantial amount of PPII in their structural ensembles. The results discussed above furthermore showed that the experimental ROA patterns do not agree with very flexible chains with average torsion angles around PPII angles ($\phi = -75°$ and $\psi = 145°$). More likely, short stretches of PPII with average angles close to $\phi = -75°$ and $\psi = 145°$ but truncated by other secondary structure elements fit better with experiment.[21]

To further study the ROA patterns associated with IDPs, here the effect of PPII mixing with other secondary structure components is therefore explored. First, the behavior in solution of IDPs is considered. The protein α-synuclein, for example, has attracted extensive scientific interest due to its central role in Parkinson's disease and related neurodegenerative diseases (termed synucleinopathies).[7,33,34] Our group reported the experimental ROA patterns of α-synuclein adopting different conformations, yet the origin of the spectral patterns of IDPs and small differences in their ROA spectra are unknown.[7] To describe the flexible structure of IDPs, multiple structural ensembles have been proposed based on NMR approaches. In Figure 5, the Ramachandran plots of three of such structural ensembles of α-synuclein are shown. All three display distinct conformational preferences.

Due to the differences in the methodology of these three studies, the Ramachandran plots of the ensembles are quite different. Yet, all three graphs show that most backbone torsion angles fluctuate in the PPII region, with the right-handed helical region also populated. The ensemble by Tóth et al. (middle) furthermore shows an important contribution of the β-strand region. On the basis of these graphs, the mixing of PPII structure with either helical or β-strand structure is explored here. To this end, the Raman and ROA spectra of HCO-Ala_7-NH_2 model peptides that differ in the ratios of PPII/helix and PPII/β-strand were computed. As before, families of 50 structures were created by defining the backbone torsion angles. To include conformational freedom in these families of structures, a standard deviation of the mean backbone angles of σ = 20 was used. Next, ensembles of 50 structures with different specified ratios of PPII/helix or PPII/β-strand were generated as visualized in the Ramachandran plots in Figures 6 and 7. To vary the ratio of the two secondary structures, we used a similar approach to that described in Scheme 1, by adding an additional step to randomly assign each residue to one of the two secondary structures, as

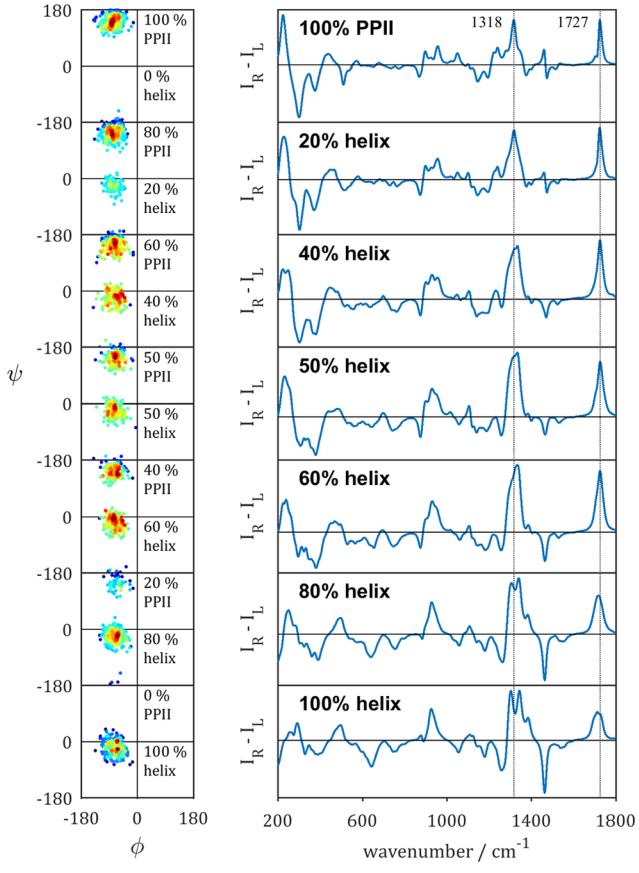

Figure 6. Mixing of PPII with right-handed helical structure: Ramachandran plots of the backbone angles of each family of 50 DFT optimized structures with a specific ratio of PPII/helix. For PPII, (−75; 145°) was used as the central pair of angles, and for the helical structures, (−71; −18°) (see Ramachandran plot for the ensemble by Schwalbe et al. in Figure 5). On the right-hand side, the ROA ($I_R - I_L$) spectra are shown as the average of 50 spectra of the 50 structures.

DOI: 10.1021/acsomega.8b01955
ACS Omega 2018, 3, 12944−12955

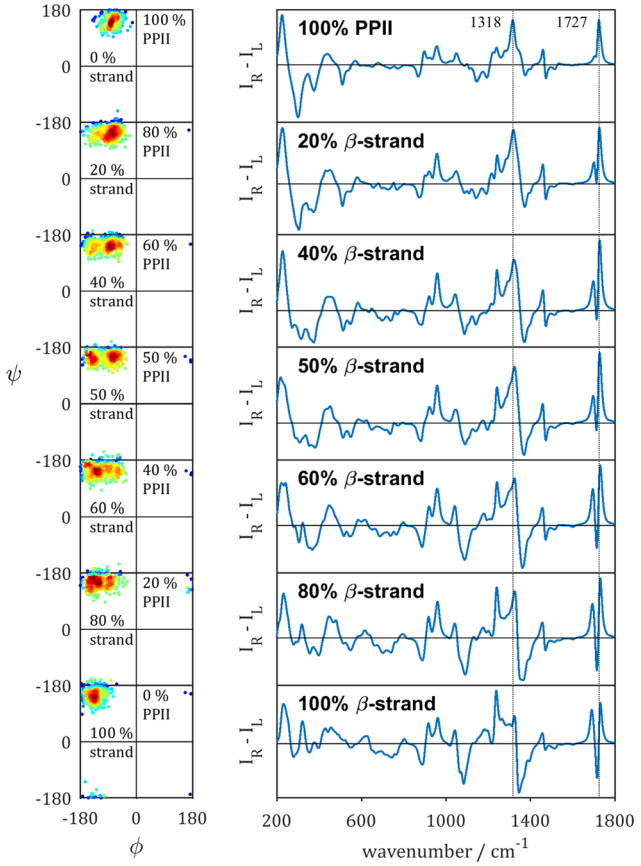

Figure 7. Mixing of PPII with β-strand structure: Ramachandran plots of the backbone angles of each family of 50 DFT optimized conformations with a specific ratio of PPII/helix. For PPII, (−75; 145°) was used as the central angles, and for the β-strand, (−125; 150°) (see Ramachandran plot for the Tóth ensemble in Figure 5). On the right-hand side, the ROA ($I_R - I_L$) spectra are shown as the average of 50 spectra of the 50 corresponding structures.

described in more detail in Scheme S1 in the Supporting Information.

In Figure 6, the average ROA spectra of the different conformational families of PPII/helix are shown (the corresponding Raman spectra are shown in Figure S6). The amide I band in both the Raman and ROA spectra shifts down about 15 cm^{-1} going from 100% PPII to 100% right-handed helix because of the presence of C═O···H−N hydrogen bonds in the helical structures. The broad amide III band around 1230−1240 cm^{-1} in the Raman spectra gradually decreases in intensity, marking the reduction in PPII content while the positive bands around 1300 and 1345 cm^{-1} increase, both arising from Cα−H bending modes coupled to amide III vibrational motions in the helical structure.

In the ROA spectra, the change in the extended amide III region is more visible with the positive band at 1318 cm^{-1} (100% PPII) becoming broader upon increasing the helical content, with eventually the appearance of the characteristic two positive bands marking α-helical structure around 1300 and 1345 cm^{-1} (100% helix). Two important conclusions can be drawn from this graph. First, the broad asymmetric band in the amide III region in the ROA spectra with mixed PPII/helix suggests that the extended amide III region in experimental ROA spectra of IDPs arises from PPII segments mixed with other structural elements such as helical structure. Second, the appearance of the two positive ROA bands marking α-helical structure at 1300 and 1345 cm^{-1} only for a content of 80−100% helix again shows that ROA is sensitive to rigid secondary structure elements in solution. As experimental ROA spectra of proteins in solution with much less helical content than 80% already show the two positive bands, these bands must arise from sequences of multiple residues adopting a right-handed helix. Since here a helix with 3_{10}-backbone angles was considered, the unfolding of an α-helix to PPII structure was calculated to further study the mixing of secondary structures.

As the Ramachandran plot of the ensemble of α-synculein by Tóth et al. shows an important population of the β-strand region (Figure 5), the effect of the mixing of PPII with β-strand structure on the ROA patterns was also probed here. Similar to the previous calculations, multiple families of 50 structures with different ratios of PPII/β-strand were generated (see the Ramachandran plot in Figure 7). As can be seen in the computed spectra of these conformational families, the amide I region is not much shifted upon variation of the PPII/β-strand ratio (the corresponding Raman spectra are shown in Figure S7). However, as can be seen in Figure 7, the ROA amide I does change shape quite distinctly, with a negative band emerging upon increasing the β-strand content. This spectral change hence arises from the change in the orientation of the C═O groups and not from hydrogen bonding.

The extended amide III region is quite sensitive to the mixing of PPII/β-strand in both the Raman and ROA spectra. A positive amide III band appears around 1240 cm^{-1} in the ROA spectra upon increasing the β-strand content, as well as a broad negative band in the region 1345−1370 cm^{-1}. The experimental ROA spectrum of, e.g., poly-L-lysine, in β-sheet state displays a broad positive band around 1260 cm^{-1} and a negative band at 1351 cm^{-1}.[36] Such a negative band is often observed in the experimental ROA spectra of proteins with a large β-sheet content.[36] While for the mixing of PPII with helical structure the skeletal stretch region changed from a typical PPII −/+/+ signature (860−980 cm^{-1}) to a positive band (930 cm^{-1}) with high helical content, this spectral pattern −/+/+ (860−980 cm^{-1}) upon mixing PPII with β-strand structure remains the same.

To conclude, the spectral features that appear in the ROA spectra in Figure 7 upon increasing the β-strand content do not reflect spectral patterns observed experimentally for IDPs. The ROA spectra of mixing PPII backbone torsion angles with helical backbone torsion angles is on the other hand reminiscent of the experimental ROA spectral patterns observed for IDPs. Finally, to further study the mixing of PPII with helical secondary structure, in the next section, the unfolding of an α-helix to a PPII backbone is studied.

α-Helix Unfolding to PPII. Above, the transition of helical structure to PPII secondary structure was probed by varying all backbone torsion angles of a peptide model simultaneously and calculating the Raman and ROA spectra at set percentages of the two secondary structures (two pairs of ϕ and ψ angles). In this section, the change in the spectra is considered when one regular α-helical model peptide makes a gradual transition to PPII extended helix by changing the backbone angles of each residue one by one starting from the N-terminus. By doing this for a HCO-(L-Ala)$_{11}$-NH_2 peptide, the difference with the results described above is that multiple consecutive residues of both secondary structure types coexist within the same peptide.

DOI: 10.1021/acsomega.8b01955
ACS Omega 2018, 3, 12944−12955

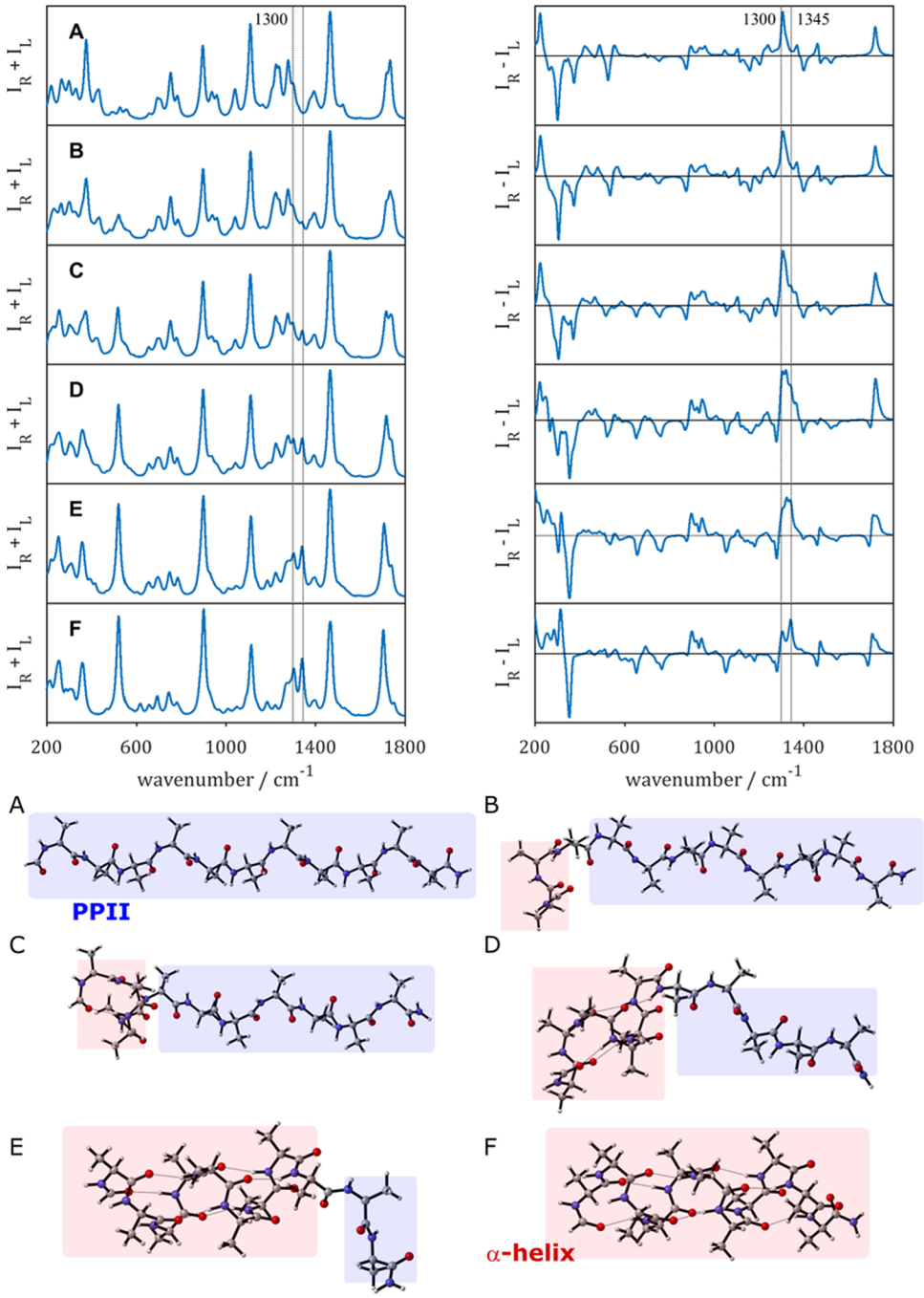

Figure 8. Raman ($I_R + I_L$) and ROA ($I_R + I_L$) spectra of the gradual change of a PPII backbone conformation to an α-helix starting from the N-terminus. Each spectrum is calculated for a HCO-Ala_{11}-NH_2 model peptide. From (A) to (F), each time the next two consecutive (ϕ; ψ) angles are changed from PPII (−75; 145°) to α-helical (−64; −41°): (A) residues 1−11 PPII, (B) residues 1−2 α-helical, (C) 1−4 α-helical, (D) 1−6 α-helical, (E) 1−8 α-helical, and (F) 1−10 α-helical.

As shown in Figure 8, upon varying the structure from 100% PPII to 100% α-helix, the largest changes in the Raman spectra appear in the 500−550 cm^{-1} region (backbone deformations and out-of-plane N−H bending), the extended amide III region, and the amide I region. The ROA spectra show considerable changes across the entire spectral window. Amide I in the ROA spectra changes from a positive band associated with PPII structure to a −/+ couplet marking α-helical structure. The most interesting spectral region appears to be the amide III region that retains a strong positive band around 1300−1325 cm^{-1}, while only for the spectrum consisting of 100% α-helical backbone, the two positive amide III bands are clearly distinguishable.

In Figure 9, the amide III spectral region is shown in more detail. There are different contributions to the extended amide III region. The vibrational modes in this spectral region arise from the coupling of C−N stretching with Cα−H and N−H bending.[32] The coupling of the latter two bending modes is very sensitive to the exact geometry and is considered one of the most important regions in the ROA spectrum due to the intense bands ca. 1230−1350 cm^{-1}.[1] In Figure 9, with higher α-helical content in the model peptide, a negative amide III

DOI: 10.1021/acsomega.8b01955
ACS Omega 2018, 3, 12944−12955

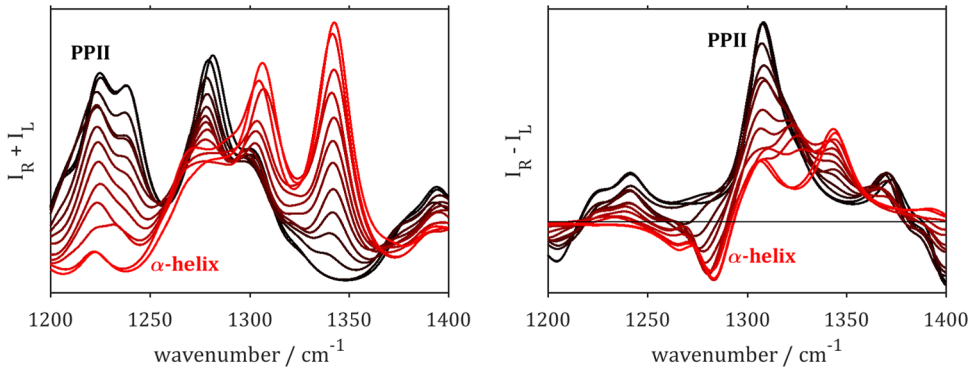

Figure 9. Raman ($I_R + I_L$) and ROA ($I_R - I_L$) spectra in the extended amide III region of HCO-(L-Ala)$_{11}$-NH$_2$ in an α-helical conformation (red) that was unfolded to a PPII backbone conformation starting from the N-terminus to an α-helix (red). Ranging from the red to the black lines, one pair of consecutive (ϕ; ψ) angles for each consecutive spectrum changed from (−75; 145°) to (−64; −41°).

band appears below 1300 cm^{-1}. Furthermore, four positive bands are observed in the Cα−H bending mode region (1300−1370 cm^{-1}). PPII structure has a prominent positive band at 1308 cm^{-1} that diminishes with increasing α-helical content. The shoulder around 1323 cm^{-1} becomes more evident for the mixed PPII/α-helical structures. Only for the fully α-helical model structure, the ROA band marking α-helical structure at 1343 cm^{-1} is separately observed without the band around 1323 cm^{-1}. The band around 1323 cm^{-1} has two important contributions: (1) amide III modes in the backbone and (2) an amide III mode of the C-terminus. The latter mode, arising from the capping of the peptide model, possibly explains the intense appearance of the band in the amide III region of the mixed PPII/α-helix structures. A fourth Cα−H bending mode band is observed around 1370 cm^{-1} for the structures with a high PPII content.

A few conclusions can be drawn from Figure 9. First, the amide III band around 1340−1345 cm^{-1} is the most reliable marker for α-helical structure. Even for a minor contribution of ϕ and ψ α-helical angles, this band is observed. It mainly arises from Cα−H bending with its motion parallel to the Cα−N bond. The diminishing of this ROA band around 1345 cm^{-1} is reminiscent of the gradual disappearing of that band in the experimental ROA spectra of thermally unfolding α-lactalbumin.[37,38] On the other hand, here, a positive intensity of around 1300−1310 cm^{-1} in the ROA spectrum is observed for both the α-helical and PPII secondary structures, and should hence be carefully assigned. Furthermore, the region 1200−1300 cm^{-1} has an important contribution from C−N stretching, which is very dependent on hydrogen bonding, e.g., with water.[39] For structures with a large content of PPII structure, intense Raman bands are observed in that region in Figure 9. However, PPII structure is not stabilized by intramolecular hydrogen bonds such as in the case of α-helical structure, rather the carbonyl groups pointing outward from the backbone allow hydrogen bonding with water.[25] This urges the need to study the effect of explicit hydration on the ROA patterns in more detail, specifically in the case of PPII structure. Also the negative ROA band around 1280 cm^{-1} appears upon hydrogen bond formation in the α-helical segment of the model peptide. Experimentally, the ROA spectra of IDPs show a negative band in this region. On the basis of the calculations in this study, there are no indications for this negative band arising from PPII secondary structure, which is the main structural element of IDPs. The calculated spectra in this study, however, show that it could arise from helical contributions.

CONCLUSIONS

This study of the effect of conformational dynamics and structural disorder showed that ROA patterns mainly reflect the average distribution of the backbone conformation. Therefore, the approach to elucidate experimental ROA spectra based on a large database of calculated spectra of fixed model structures reported before by our group is a good simple methodology to study the amide modes.[10] Only upon larger variation of the backbone angles of common secondary structure elements such as PPII and right-handed helical structure, the ROA patterns average.

This study furthermore supports the view that experimental ROA patterns likely stem from the most rigid components in the structural ensemble. For example, in the case of IDPs, a strong positive band ∼1318 cm^{-1} in the amide III reflects PPII secondary structure with backbone angles close (variation of the mean angles $\sigma \leq 20°$) to the average PPII backbone angles ($\phi = -75°$ and $\psi = 145°$), rather than a fully flexible structure with the mean backbone angles being $\phi = -75°$ and $\psi = 145°$. Furthermore, the mixing of PPII with other secondary structure elements may explain the experimentally observed ROA patterns. Mixing of PPII structure with right-handed helical structure is more alike experimental ROA patterns than mixing with β-strand structure. Furthermore, it was shown that ROA is extremely sensitive to the exact conformation of α-helical structure and the tilt of the carbonyl groups in the C═O···H−N hydrogen bonds, which could be affected by explicit hydrogen bonding with water.[10] Also the CH and CH$_2$ groups in amino acid side chains could have a pronounced effect on, e.g., the amide III region through coupling of the vibrational modes of these groups with Cα−H and N−H bending modes, which will hence be the focus of our future research.

METHODOLOGY

ROA signals of proteins mainly arise from the amide and skeletal stretching vibrations in the backbone; therefore, poly-L-alanine peptides are often used in computational ROA studies, since this is the smallest chiral amino acid and conformational averaging of the side chains does not need to be considered.[10] In this study, model peptide structures of the general formula HCO-(L-Ala)$_7$-NH$_2$ were created using the Python peptide builder by Tien et al. that generates the models based on a set of ϕ and ψ torsion angles.[40] First, different

DOI: 10.1021/acsomega.8b01955
ACS Omega 2018, 3, 12944−12955

secondary structure element models were created by selecting specific pairs of torsion angles (step 1 in Scheme 1) and setting all backbone ϕ and ψ angles to this pair for each residue in the peptide (step 2 in Scheme 1). In that way, "regular" conformations are generated. To include conformational dynamics, the model ϕ and ψ angles were varied to different extents from the initial angles (step 3 in Scheme 1). To this end, the torsion angles of each residue were generated using the "randn" function in Matlab R2017a (Mathworks, Inc.) that renders normally distributed pseudorandom numbers with standard deviation 1 (see curve in Scheme 1). By increasing the standard deviation of these random numbers, the generated ϕ and ψ angles deviate more and more from the initial chosen angles, and hence more and more conformational variation is imposed on the model peptide. In this way, families of 50 randomly generated conformations were constructed, where for each family, a different degree of conformational freedom was imposed by multiplying the chosen standard deviation σ of the torsion angles 6, 10, 20, or 30° with a normally distributed random number (step 3 in Scheme 1). So, for each backbone angle of each conformation, a new random number was generated.

Next, the geometry of each conformation of the model peptide was partially optimized using the normal mode optimization procedure.[41] By locking the normal modes between i300 cm^{-1} (imaginary) and 300 cm^{-1} in the optimization, the backbone conformation is retained, while the modes of spectroscopic interest are fully relaxed.[41] These geometry optimizations were performed using the B3PW91 DFT functional and the 6-31G(d,p) basis set. Subsequently, the Hessian matrix and Raman and ROA tensors were calculated using the same functional and the 6-31++G(d,p) basis set. The experimental backscattered Raman ($I_R + I_L$) and ROA ($I_R - I_L$) spectral shapes were simulated by using a Lorentzian function for each normal mode with a full width at half-height of 20 cm^{-1} to mimic the physical line broadening in the experimental spectra. A Boltzmann intensity correction factor was applied for a temperature of 300 K (see, e.g., Cheeseman et al.).[42] Solvent−solute interactions with water were taken into account using the conductor-like polarizable continuum model with the default solvent parameters in the program Gaussian. For all DFT calculations, the Gaussian 16 (rev A.03) program was used.[43] For the sake of comparison with experimental data in the scientific literature, the calculated spectra are scaled in the wavenumber dimension by using a global scaling factor of 0.987.[10] Images of molecular structures were created using Jmol-12.2.32 or CylView v1.0 β, and figures were produced using Matlab R2017a.[44,45] The Ramachandran plots were prepared with "scatplot" in Matlab.

■ ASSOCIATED CONTENT

Supporting Information

The Supporting Information is available free of charge on the ACS Publications website at DOI: 10.1021/acsomega.8b01955.

Raman and ROA spectra of the separate conformations of the mean spectra shown in Figure 3; Raman spectra computed for the conformations of the ROA spectra shown in Figures 6 and 7 (PDF)

■ AUTHOR INFORMATION

Corresponding Author

*E-mail: christian.johannessen@uantwerpen.be. Phone: +32 3 265 35 05. Fax: +32 3 265 32 33.

ORCID

Carl Mensch: 0000-0003-3028-2785

Christian Johannessen: 0000-0003-2613-9476

Notes

The authors declare no competing financial interest.

■ ACKNOWLEDGMENTS

The authors acknowledge the Flemish Supercomputing Centre (VSC) for providing computing resources and support. C.M. acknowledges the University of Antwerp for funding his research. Furthermore, C.M. thanks Profs. Malene Ringkjøbing Jensen and Michele Vendruscolo for providing the α-synuclein ensembles. Financial support by the BOF concerted research action "4D protein structure" is acknowledged.

■ ABBREVIATIONS

ROA, Raman optical activity; IDP, intrinsically disordered protein; DFT, density functional theory; PPII, poly-L-proline type II helix; NMR, nuclear magnetic resonance

■ REFERENCES

(1) Barron, L. D.; Hecht, L.; Blanch, E. W.; Bell, A. F. Solution Structure and Dynamics of Biomolecules from Raman Optical Activity. *Prog. Biophys. Mol. Biol.* **2000**, *73*, 1−49.

(2) Barron, L. D. The Development of Biomolecular Raman Optical Activity Spectroscopy. *Biomed. Spectrosc. Imaging* **2015**, *4*, 223−253.

(3) Hudecová, J.; Kapitán, J.; Baumruk, V.; Hammer, R. P.; Keiderling, T. A.; Bouř, P. Side Chain and Flexibility Contributions to the Raman Optical Activity Spectra of a Model Cyclic Hexapeptide. *J. Phys. Chem. A* **2010**, *114*, 7642−7651.

(4) Mensch, C.; Pendrill, R.; Widmalm, G.; Johannessen, C. Studying the Glycan Moiety of RNase B by Means of Raman and Raman Optical Activity. *ChemPhysChem* **2014**, *15*, 2252−2254.

(5) Johannessen, C.; Pendrill, R.; Widmalm, G.; Hecht, L.; Barron, L. D. Glycan Structure of a High-Mannose Glycoprotein from Raman Optical Activity. *Angew. Chem., Int. Ed.* **2011**, *50*, 5349−5351.

(6) Van de Vondel, E.; Mensch, C.; Johannessen, C. Direct Measurements of the Crowding Effect in Proteins by Means of Raman Optical Activity. *J. Phys. Chem. B* **2016**, *120*, 886−890.

(7) Mensch, C.; Konijnenberg, A.; Van Elzen, R.; Lambeir, A.-M.; Sobott, F.; Johannessen, C. Raman Optical Activity of Human α-Synuclein in Intrinsically Disordered, Micelle-Bound α-Helical, Molten Globule and Oligomeric β-Sheet State. *J. Raman Spectrosc.* **2017**, *48*, 910−918.

(8) Uversky, V. N. A Decade and a Half of Protein Intrinsic Disorder: Biology Still Waits for Physics. *Protein Sci.* **2013**, *22*, 693−724.

(9) Wilson, G.; Hecht, L.; Barron, L. D. Residual Structure in Unfolded Proteins Revealed by Raman Optical Activity. *Biochemistry* **1996**, *35*, 12518−12525.

(10) Mensch, C.; Barron, L. D.; Johannessen, C. Ramachandran Mapping of Peptide Conformation Using a Large Database of Computed Raman and Raman Optical Activity Spectra. *Phys. Chem. Chem. Phys.* **2016**, *18*, 31757−31768.

(11) Johannessen, C.; Blanch, E. W. Recent Developments In Raman Optical Activity Calculations On Biomolecules (Mini-Review). *Curr. Phys. Chem.* **2013**, *3*, 140−150.

(12) Ostovar pour, S.; Barron, L. D.; Mutter, S. T.; Blanch, E. W. Raman Optical Activity. *Chiral Analysis*; Elsevier, 2018; pp 249−291.

(13) Yamamoto, S.; Straka, M.; Watarai, H.; Bouř, P. Formation and Structure of the Potassium Complex of Valinomycin in Solution

DOI: 10.1021/acsomega.8b01955
ACS Omega 2018, 3, 12944−12955

Studied by Raman Optical Activity Spectroscopy. *Phys. Chem. Chem. Phys.* **2010**, *12*, 11021.
(14) Yamamoto, S.; Watarai, H.; Bouř, P. Monitoring the Backbone Conformation of Valinomycin by Raman Optical Activity. *ChemPhysChem* **2011**, *12*, 1509−1518.
(15) Yamamoto, S.; Kaminský, J.; Bouř, P. Structure and Vibrational Motion of Insulin from Raman Optical Activity Spectra. *Anal. Chem.* **2012**, *84*, 2440−2451.
(16) Kessler, J.; Kapitán, J.; Bouř, P. First-Principles Predictions of Vibrational Raman Optical Activity of Globular Proteins. *J. Phys. Chem. Lett.* **2015**, *6*, 3314−3319.
(17) Kessler, J.; Yamamoto, S.; Bouř, P. Establishing the Link between Fibril Formation and Raman Optical Activity Spectra of Insulin. *Phys. Chem. Chem. Phys.* **2017**, *19*, 13614−13621.
(18) Luber, S.; Reiher, M. Theoretical Raman Optical Activity Study of the β Domain of Rat Metallothionein. *J. Phys. Chem. B* **2010**, *114*, 1057−1063.
(19) Jacob, C. R.; Luber, S.; Reiher, M. Understanding the Signatures of Secondary-Structure Elements in Proteins with Raman Optical Activity Spectroscopy. *Chem. − Eur. J.* **2009**, *15*, 13491−13508.
(20) Herrmann, C.; Ruud, K.; Reiher, M. Can Raman Optical Activity Separate Axial from Local Chirality? A Theoretical Study of Helical Deca-Alanine. *ChemPhysChem* **2006**, *7*, 2189−2196.
(21) Zhu, F.; Kapitan, J.; Tranter, G. E.; Pudney, P. D. A.; Isaacs, N. W.; Hecht, L.; Barron, L. D. Residual Structure in Disordered Peptides and Unfolded Proteins from Multivariate Analysis and Ab Initio Simulation of Raman Optical Activity Data. *Proteins: Struct., Funct., Bioinf.* **2008**, *70*, 823−833.
(22) Yamamoto, S.; Furukawa, T.; Bouř, P.; Ozaki, Y. Solvated States of Poly- L-Alanine α-Helix Explored by Raman Optical Activity. *J. Phys. Chem. A* **2014**, *118*, 3655−3662.
(23) Weymuth, T.; Reiher, M. Characteristic Raman Optical Activity Signatures of Protein β-Sheets. *J. Phys. Chem. B* **2013**, *117*, 11943−11953.
(24) Luber, S. Solvent Effects in Calculated Vibrational Raman Optical Activity Spectra of α-Helices. *J. Phys. Chem. A* **2013**, *117*, 2760−2770.
(25) Adzhubei, A. A.; Sternberg, M. J. E.; Makarov, A. A. Polyproline-II Helix in Proteins: Structure and Function. *J. Mol. Biol.* **2013**, *425*, 2100−2132.
(26) Barron, L. D.; Zhu, F.; Hecht, L.; Tranter, G. E.; Isaacs, N. W. Raman Optical Activity: An Incisive Probe of Molecular Chirality and Biomolecular Structure. *J. Mol. Struct.* **2007**, *834*−*836*, 7−16.
(27) Blanch, E. W.; Morozova-Roche, L. A.; Cochran, D. A. E.; Doig, A. J.; Hecht, L.; Barron, L. D. Is Polyproline II Helix the Killer Conformation? A Raman Optical Activity Study of the Amyloidogenic Prefibrillar Intermediate of Human Lysozyme. *J. Mol. Biol.* **2000**, *301*, 553−563.
(28) Schweitzer-Stenner, R.; Measey, T. J. The Alanine-Rich XAO Peptide Adopts a Heterogeneous Population, Including Turn-like and Polyproline II Conformations. *Proc. Natl. Acad. Sci. U.S.A.* **2007**, *104*, 6649−6654.
(29) Zagrovic, B.; Lipfert, J.; Sorin, E. J.; Millett, I. S.; van Gunsteren, W. F.; Doniach, S.; Pande, V. S. Unusual Compactness of a Polyproline Type II Structure. *Proc. Natl. Acad. Sci. U.S.A.* **2005**, *102*, 11698−11703.
(30) Blanch, E. W.; Bell, A. F.; Hecht, L.; Day, L. A.; Barron, L. D. Raman Optical Activity of Filamentous Bacteriophages: Hydration of α-Helices. *J. Mol. Biol.* **1999**, *290*, 1−7.
(31) Blanch, E. W.; Hecht, L.; Day, L. A.; Pederson, D. M.; Barron, L. D. Tryptophan Absolute Stereochemistry in Viral Coat Proteins from Raman Optical Activity. *J. Am. Chem. Soc.* **2001**, *123*, 4863−4864.
(32) Jacob, C. R.; Reiher, M. Localizing Normal Modes in Large Molecules. *J. Chem. Phys.* **2009**, *130*, No. 084106.
(33) Tóth, G.; Gardai, S. J.; Zago, W.; Bertoncini, C. W.; Cremades, N.; Roy, S. L.; Tambe, M. A.; Rochet, J.-C.; Galvagnion, C.; Skibinski, G.; Finkbeiner, S.; Bova, M.; Regnstrom, K.; Chiou, S.-S.; Johnston, J.; Callaway, K.; Anderson, J. P.; Jobling, M. F.; Buell, A. K.; Yednock, T. A.; Knowles, T. P. J.; Vendruscolo, M.; Christodoulou, J.; Dobson, C. M.; Schenk, D.; McConlogue, L. Targeting the Intrinsically Disordered Structural Ensemble of α-Synuclein by Small Molecules as a Potential Therapeutic Strategy for Parkinson's Disease. *PLoS One* **2014**, *9*, No. e87133.
(34) Allison, J. R.; Varnai, P.; Dobson, C. M.; Vendruscolo, M. Determination of the Free Energy Landscape of α-Synuclein Using Spin Label Nuclear Magnetic Resonance Measurements. *J. Am. Chem. Soc.* **2009**, *131*, 18314−18326.
(35) Schwalbe, M.; Ozenne, V.; Bibow, S.; Jaremko, M.; Jaremko, L.; Gajda, M.; Jensen, M. R.; Biernat, J.; Becker, S.; Mandelkow, E.; Zweckstetter, M.; Blackledge, M. Predictive Atomic Resolution Descriptions of Intrinsically Disordered HTau40 and α-Synuclein in Solution from NMR and Small Angle Scattering. *Structure* **2014**, *22*, 238−249.
(36) McColl, I. H.; Blanch, E. W.; Gill, A. C.; Rhie, A. G. O.; Ritchie, M. A.; Hecht, L.; Nielsen, K.; Barron, L. D. A New Perspective on Beta-Sheet Structures Using Vibrational Raman Optical Activity: From Poly(L-Lysine) to the Prion Protein. *J. Am. Chem. Soc.* **2003**, *125*, 10019−10026.
(37) Wilson, G.; Ford, S. J.; Cooper, A.; Hecht, L.; Wen, Z. Q.; Barron, L. D. Vibrational Raman Optical Activity of α-Lactalbumin: Comparison with Lysozyme, and Evidence for Native Tertiary Folds in Molten Globule States. *J. Mol. Biol.* **1995**, *254*, 747−760.
(38) Wilson, G.; Hecht, L.; Barron, L. D. The Native-like Tertiary Fold in Molten Globule α-Lactalbumin Appears to Be Controlled by a Continuous Phase Transition. *J. Mol. Biol.* **1996**, *261*, 341−347.
(39) Myshakina, N. S.; Ahmed, Z.; Asher, S. A. Dependence of Amide Vibrations on Hydrogen Bonding. *J. Phys. Chem. B* **2008**, *112*, 11873−11877.
(40) Tien, M. Z.; Sydykova, D. K.; Meyer, A. G.; Wilke, C. O. PeptideBuilder: A Simple Python Library to Generate Model Peptides. *PeerJ* **2013**, *1*, No. e80.
(41) Bouř, P.; Keiderling, T. A. Partial Optimization of Molecular Geometry in Normal Coordinates and Use as a Tool for Simulation of Vibrational Spectra. *J. Chem. Phys.* **2002**, *117*, 4126−4132.
(42) Cheeseman, J. R.; Shaik, M. S.; Popelier, P. L. A.; Blanch, E. W. Calculation of Raman Optical Activity Spectra of Methyl-β-D-Glucose Incorporating a Full Molecular Dynamics Simulation of Hydration Effects. *J. Am. Chem. Soc.* **2011**, *133*, 4991−4997.
(43) Frisch, M. J.; Trucks, G. W.; Schlegel, H. B.; Scuseria, G. E.; Robb, M. A.; Cheeseman, J. R.; Scalmani, G.; Barone, V.; Petersson, G. A.; Nakatsuji, H.; Li, X.; Caricato, M.; Marenich, A. V.; Bloino, J.; Janesko, B. G.; Gomperts, R.; Mennucci, B.; Hratchian, H. P.; Ortiz, J. V.; Izmaylov, A. F.; Sonnenberg, J. L.; Williams-Young, D.; Ding, F.; Lipparini, F.; Egidi, F.; Goings, J.; Peng, B.; Petrone, A.; Henderson, T.; Ranasinghe, D.; Zakrzewski, V. G.; Gao, J.; Rega, N.; Zheng, G.; Liang, W.; Hada, M.; Ehara, M.; Toyota, K.; Fukuda, R.; Hasegawa, J.; Ishida, M.; Nakajima, T.; Honda, Y.; Kitao, O.; Nakai, H.; Vreven, T.; Throssell, K., Jr.; Montgomery, J. A.; Peralta, J. E.; Ogliaro, F.; Bearpark, M. J.; Heyd, J. J.; Brothers, E. N.; Kudin, K. N.; Staroverov, V. N.; Keith, T. A.; Kobayashi, R.; Normand, J.; Raghavachari, K.; Rendell, A. P.; Burant, J. C.; Iyengar, S. S.; Tomasi, J.; Cossi, M.; Millam, J. M.; Klene, M.; Adamo, C.; Cammi, R.; Ochterski, J. W.; Martin, R. L.; Morokuma, K.; Farkas, O.; Foresman, J. B.; Fox, D. J. *Gaussian 16*, revision A.03; Gaussian, Inc.: Wallingford, CT, 2016.
(44) *Jmol: An Open-Source Java Viewer for Chemical Structures in 3D*, 2012. http://www.Jmol.Org/ (accessed Nov 12, 2012).
(45) *CYLview: Visualization and Analysis Software for Computational Chemistry*, 2018. http://www.Cylview.Org/ (accessed April 23, 2018).

DOI: 10.1021/acsomega.8b01955
ACS Omega 2018, 3, 12944−12955